Chemistry Europe
European Chemical Societies Publishing

WILEY VCH

Excellence in Chemistry Research

Announcing our new flagship journal

- Gold Open Access
- Publishing charges waived
- Preprints welcome
- Edited by active scientists

Meet the Editors of *ChemistryEurope*

Luisa De Cola
Università degli Studi di Milano Statale, Italy

Ive Hermans
University of Wisconsin-Madison, USA

Ken Tanaka
Tokyo Institute of Technology, Japan

Chemistry–A European Journal
Research Article
doi.org/10.1002/chem.202301854
Chemistry Europe
European Chemical Societies Publishing
www.chemeurj.org

Hot Paper

Special Collection

Chemical Tailoring of β-Cyclodextrin-Graphene Oxide for Enhanced Per- and Polyfluoroalkyl Substances (PFAS) Adsorption from Drinking Water

Francesca Tunioli[+],[a] Tainah D. Marforio[+],[b] Laura Favaretto,[a] Sebastiano Mantovani,[a] Angela Pintus,[a] Antonio Bianchi,[a] Alessandro Kovtun,[a] Marco Agnes,[a] Vincenzo Palermo,[a, c] Matteo Calvaresi,[b] Maria Luisa Navacchia,[a] and Manuela Melucci*[a]

Dedicated to Prof. Maurizio Prato on the occasion of his 70th birthday.

We report on the synthesis of β-cyclodextrin (βCD) modified graphene oxide (GO) nanosheets, having different sized alkyl linkers (GO-C_n-βCD) and their exploitation as sorbent of per- and polyfluoroalkyl substances (PFAS) from drinking water. βCD were functionalized with a pending amino group, and the resulting precursors grafted to GO nanosheets by epoxide ring opening reaction. Loading of βCD units in the range 12%–36% was estimated by combined XPS and elemental analysis. Adsorption tests on perfluorobutanoic acid (PFBA), a particularly persistent PFAS selected as case study, revealed a strong influence of the alkyl linker length on the adsorption efficiency, with the hexyl linker derivative GO-C_6-βCD outperforming both pristine GO and granular activated carbon (GAC), the standard sorbent benchmark. Molecular dynamic simulations ascribed this evidence to the favorable orientation of the βCD unit on the surface of GO which enables a strong contaminant molecules retention.

Introduction

Per- and polyfluoroalkyl substances (PFAS), also known as *forever chemicals*, are currently subject of global concern for their massive use in every-day products, their persistency in the environment and human bodies, and proved eco- and human toxicity.[1] PFAS are nowadays used in hundreds of thousands of industrial products for food packaging, non-stick cookware, paints, waterproof clothing, stain repellent, cosmetics, and firefighting foams. The disposal of such products or their wastes leads to the release of PFAS and their accumulation in different environmental compartments, including water bodies.[2]

Surprisingly, recent studies have shown that toilet paper is one of the major sources of PFAS entering wastewater treatment systems, contributing to the introduction of up to 80 μg/person-year, corresponding to 60 kg/year only in Europe, of 6:2 fluorotelomer phosphate diester (6:2 diPAP) in wastewaters.[3]

Given the resistance of this class of molecules to current water treatment technologies, PFAS occurrence in drinking water has been reported in several areas, such as the Italian Northern region of Veneto[4] or in southern Sweden, where residents showed PFAS blood levels 100 times higher than the reference group.[5]

Adsorption on granular activated carbon (GAC) is one of the most common strategies for PFAS removal.[6] However, GAC performances are strongly related to the carbon-chain length of PFAS.[7] Short chain PFAS (i.e., PFAS with eight or fewer carbon atoms),[8] which include perfluorobutanoic acid (PFBA), have higher water solubility,[7a] and therefore they are adsorbed to a lesser extent by GAC in the operational conditions used in potabilization plant (i.e., average contact time of 10–20 min).[2a,9]

In addition, a fast drop of initial adsorption performance of GAC from 100% to 20% has been documented for short chain PFAS in real water treatment plants.[10]

Recently, the suitability of graphene oxide (GO) and its derivatives on the removal of emerging contaminants from drinking water has been widely documented.[11]

[a] F. Tunioli,[+] L. Favaretto, S. Mantovani, A. Pintus, Dr. A. Bianchi, Dr. A. Kovtun, Dr. M. Agnes, Dr. V. Palermo, Dr. M. L. Navacchia, Dr. M. Melucci
Institute for Organic Synthesis and Photoreactivity (ISOF)
Consiglio Nazionale delle Ricerche (CNR)
Via Gobetti 101, 40129, Bologna, BO (Italy)
E-mail: manuela.melucci@isof.cnr.it

[b] Dr. T. D. Marforio,[+] Prof. Dr. M. Calvaresi
Department of Chemistry "G. Ciamician"
Alma Mater Studiorum – University of Bologna
Via Selmi 2, 40126, Bologna, BO (Italy)

[c] Dr. V. Palermo
Department of Industrial and Materials Science
Chalmers University of Technology
41258, Göteborg (Sweden)

[+] These authors contributed equally to this work.

Supporting information for this article is available on the WWW under https://doi.org/10.1002/chem.202301854

This article is part of a joint Special Collection in honor of Maurizio Prato.

In particular, our group demonstrated GO high adsorption capacity of PFAS (C > 5) by using GO nanosheets[12] and GO-doped[13] or coated[14] hollow fiber membranes. The adsorption on GO nanosheets was mainly related to the van der Waals interaction, which depends on hydrophobicity and thus on the perfluoroalkyl chain size of these molecules. For short-chain PFAS, such as PFBA, the negative charges of both PFAS and GO overcome hydrophobic interactions, consequently lowering the adsorption capacity of GO.[12b,13a]

Here, aiming at enhancing the interaction capability between short-chain PFAS and GO, we report on the covalent modification of GO with β-cyclodextrin units (βCD). βCD, having seven glucose units in its structure, has already proved high removal capability toward several emerging contaminants, including PFAS, through the ability to form a stable host–guest complex.[15] Indeed, PFAS can enter the cavity of βCD due to the complementary cross-sectional sizes (28 Å^2 for PFAS and 30 Å^2 for βCD) and create a stable host-guest complex where the dominant force is the hydrophobic interaction between the fluorinated PFAS chain and the βCD cavity.[16]

Here, we report on the synthesis and full characterization of a class of GO functionalized with βCD bearing differently sized alkyl linkers between GO and the βCD units. We also report on the study of their adsorption of PFBA from tap water, in comparison to pristine GO and GAC (the industrial sorbent benchmark).

Adsorption-structure relationships investigation through molecular dynamic simulations were also performed for a deeper understanding of the working mechanism driving the PFBA capture.

Results and Discussion

Synthesis and characterization

The synthesis of GO derivatives was achieved by epoxide ring opening reaction, starting from amino-ending βCD.[17] Amino-ending βCD precursors synthesis involves the preparation of mono tosyl and azide intermediates from commercially available βCD (Scheme 1a). Following published procedures,[18] amino alkyl pendants of different length, i.e., (C_0) and three different diamino-alkyl linkers, 1,2-ethylenediamine (C_2), 1,6-hexamethylenediamine (C_6), and 1,12-dodecanediamine (C_{12}) were selected to tailor the distance between the βCD unit and GO nanosheets. NMR characterization of the C_n-βCD derivatives was achieved, and data are reported in Supporting Information (Section 1). The modified amino-ending βCD were then grafted through epoxide ring opening reaction to give GO-C_n-βCD derivatives (Scheme 1b). Two control samples were prepared under the same reaction conditions using commercial βCD (without amino-alkyl linker) (GO@βCD) and without the addition of βCD (GO-control). Purification of crude materials was performed by microfiltration on Plasmart modules (Medica Spa), according to previously reported conditions.[12d]

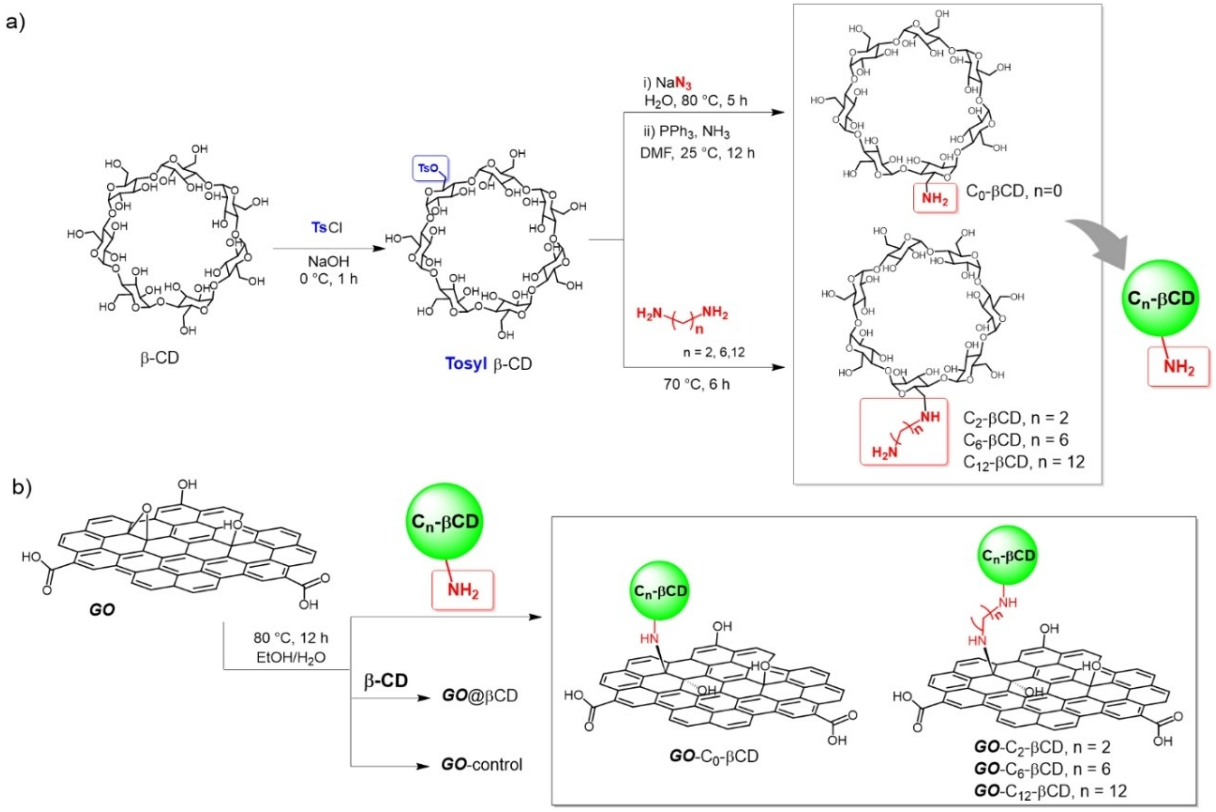

Scheme 1. Synthetic routes to a) amino-ended βCD (NH_2–C_n–βCD), and b) targeted GO–C_n–βCD and control samples: GO@βCD and GO-control.

Figure 1 shows the attenuated total reflection infrared (ATR-FTIR) spectra of GO-C_6-βCD, taken as a case study. Every GO derivatives showed the typical peaks of pristine GO (O—H stretching vibrations) at 3700–3000 cm^{-1} and that typical of βCD at 2920 cm^{-1} (C–H stretching vibrations)[19] (Figure S1, Supporting Information), confirming the presence of βCD in each modified GO. Contrarily, the spectrum of the control material GO@βCD showed only the fingerprint of pristine GO (Figure 1), confirming that, in our experimental conditions, βCD without amino pendants did not react with GO.

Accordingly, thermogravimetric analysis (TGA) of each GO-C_n-βCD revealed the presence of an inflection point at 300 °C (peak in derivative) ascribed to βCD and absent in pristine GO and in the control material GO@βCD (Figure 2, and Figure S2, Supporting Information).

The chemical structure and the βCD loading of the GO derivatives were estimated by X-ray photoelectron spectroscopy (XPS) and elemental analysis (EA).

The XPS survey spectra are showed in Figures 3a and S3a, and the atomic compositions of GO and each modified GO are reported in Table 1. The analysed materials were mainly composed of carbon, oxygen, and nitrogen, associated with i) the aromatic sp^2 regions of GO, ii) the C–O/C=O functional groups, and iii) the nitrogen functional groups (C–N) present in the modified βCD. The effective covalent functionalization of

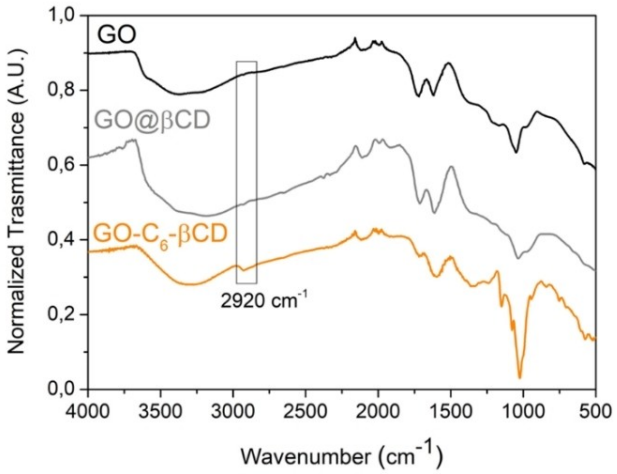

Figure 1. ATR-FTIR spectra of GO (black), GO-C_6-βCD (orange) and GO@βCD (grey).

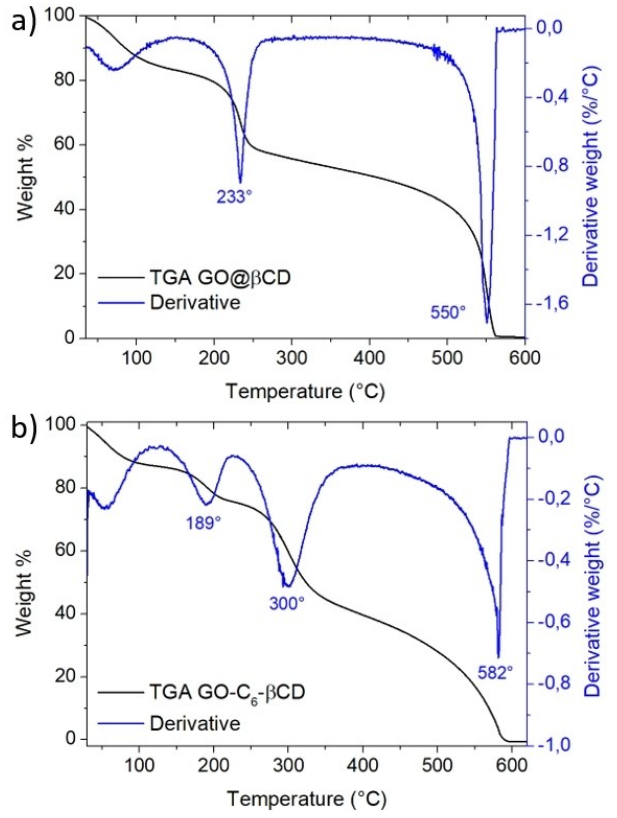

Figure 2. TGA of a) GO@βCD, and b) GO-C_6-βCD.

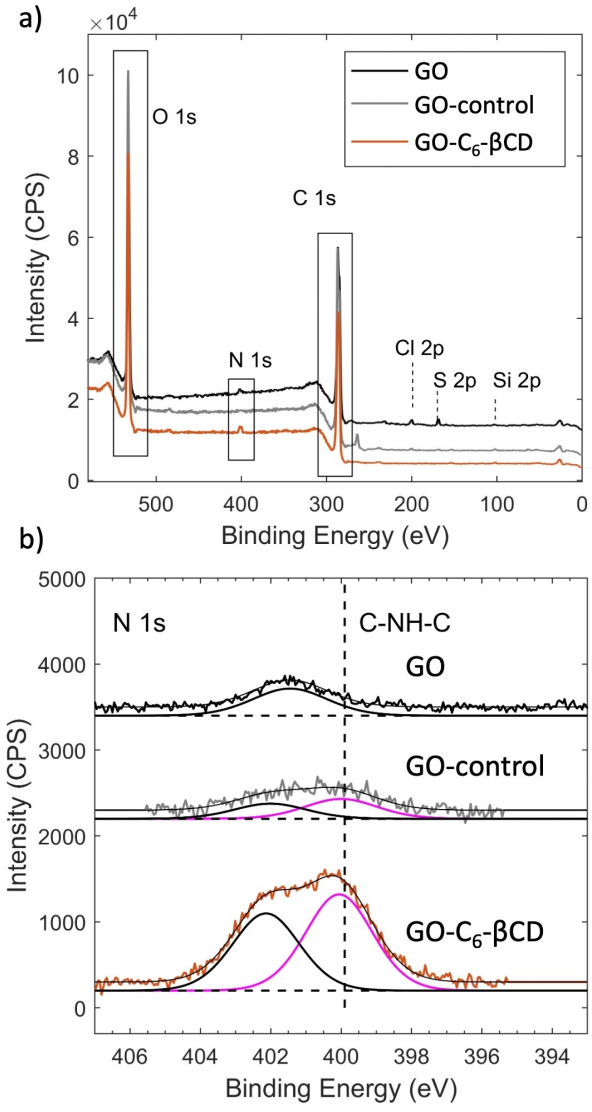

Figure 3. a) XPS survey spectra and b) N 1s signals of GO (black), GO-control (grey) and GO-C_6-βCD (orange). N 1s was fitted by two Voigt curves with binding energies at: i) 400.0 eV (C–NH–C, magenta line) and ii) 402.0 eV (other N atoms, black line). All spectra were shifted for better visualization.

Table 1. Atomic composition of βCD modified GO obtained by XPS. Errors on C (285 eV) and O (532 eV) were about ± 0.9%, and errors on N were about ± 0.1%. S and Cl were present in GO in low quantities (< 1%) and almost absent in GO-C_n-βCD (< 0.1%). Si and Na was present in low quantities (< 0.5%).

	Atomic composition [%]					
Materials	C	O	N[a]	N[b]	O/C ratio	Loading %
GO	70.4	27.0	0.7	–	0.38	–
GO-control	67.9	31.0	0.1	0.1	0.46	–
GO@βCD	70.0	29.4	0.2	0.2	0.42	–
GO-C_0-βCD	67.3	31.9	0.2	0.3	0.47	12
GO-C_2-βCD	66.0	32.0	0.5	1.0	0.48	36
GO-C_6-βCD	67.1	31.0	0.6	0.7	0.46	24
GO-C_{12}-βCD	69.1	27.8	1.1	0.8	0.40	28

[a] N signal at 402 eV. [b] N signal at 400 eV.

GO is proved by N 1s signal (Figures 3b and S3b), which was fitted by using two Voigt curves centred at 400.0 eV for C–NH–C group, associated to epoxide ring opening reaction, and at 402–401.5 eV for the other C–N groups. Unfortunately, the C–NH_2 group, which can be associated to unreacted primary amine, presents a broad assignment in literature: from 402 eV region in dopamine[20] or polydopamine[21] to 400 eV in amino acids,[22] contrarily to the well-established association of 400–400.5 eV signal to C–NH–C, also present in wide XPS polymer literature, as polyamic acid,[23] polydopamine[24] or nylon.[25] Moreover, the pristine GO presents a signal at 401.5 eV, which makes the exact association of 402–401 eV region to a specific functional group ambiguous. The N signal in pristine GO could be ascribed to nitrogen reagents used for GO production and it is reported in literature as graphitic nitrogen.[26]

For the sake of simplicity and in order to have a rough estimation of the C_n-βCD fraction in the whole GO-C_n-βCD, the loading was calculated from the N 1s peak at 400 eV, which is absent in pristine GO and present only as residual of 0.1% in the control sample (GO-control). The atomic percentage of nitrogen (%N 1s) was associated to the number of nitrogen atoms present in C_n-βCD samples. After subtracting the %N of the control material (0.1%) from the N 1s signal at 400 eV of each GO-C_n-βCD in order to consider only the N from C_n-βCD, the loading was estimated calculating the correspondent N:(N + C + O) atom ratio present in the C_n-βCD moiety, which is: 1 N:(1 N + 42 C + 34 O) for C_0-βCD; 2 N:(2 N + 44 C + 34 O) for C_2-βCD; 2 N:(2 N + 48 C + 34 O) for C_6-βCD; 2 N:(2 N + 54 C + 34 O) for C_{12}-βCD. These proportions were used to obtain an indicative estimation of C_n-βCD loading and the results are reported in Table 1. Each modified GO were found to span between 12 and 36% loading range. The oxidation degree of the studied materials was determined using the O/C ratio (Table 1). The pristine GO and the reference material (GO-control) showed an O/C ratio between the expected interval (0.38 and 0.46, respectively), proving that the experimental conditions used to bind βCD did not lead to the reduction of GO nanosheets. All the GO derivatives showed an O/C ratio comparable to pristine GO (ranging from 0.40 to 0.48), with values that monotonically decreased as the n in C_n aliphatic chain rises from 0 to 12. In the modified materials, the O/C ratio is given by the oxidation degree of the GO nanosheets, which is assumed here to be constant, and the oxidation degree of the modified C_n-βCD, which decreases as the length of the alkyl chain increases (Table S2, Supporting Information).

Moreover, the C 1s signal (Figure S4, Supporting Information) of GO-C_n-βCD presents a similar shape to that of pristine GO, which is mainly characterized by the presence of aliphatic and aromatic C–C/C=C carbons under the peak in 285 eV region and the different C–O groups present in 286–287 eV region (mainly epoxy/hydroxyl groups for GO and ether/hydroxyl groups for βCD). Combining all of the considerations above, we can conclude that the oxidation degree and the chemical structure of GO-C_n-βCD can be considered as the simple combination of the two reagents, knowing that the epoxy ring opening usually does not affect the overall amount of oxygen.

EA on modified βCD and modified GO was used to determine the bulk composition. The atomic composition (C, H, N, S, O) of each material was in good accordance with that estimated by XPS, and is reported in Tables S1 and S2, Supporting Information. In the modified C_n-βCD, the element content percentage was in good agreement with the expected one from the molecular structure (Table S1, Supporting Information). After the functionalization of GO, the amount of N consistently increases with respect to GO-control, which was taken as reference instead of GO, since it was subjected to the same reaction conditions and further purification used for modified GO.

The N% was used to obtain an indicative estimation of C_n-βCD loading (20% for GO-C_0-βCD, 32% for GO-C_2-βCD, 26% for GO-C_6-βCD, 37% for GO-C_{12}-βCD) and the results are in good agreement with XPS estimation (Table 1). The oxidation degree of GO-C_n-βCD obtained from EA presents the same monotonic trend observed by XPS: O/C ratio decreased from 0.91 to 0.66 as n in aliphatic chain C_n rises from 0 to 12 (Table S2, Supporting Information). The observed O/C ratio was systematically overestimated by EA with respect to XPS. This difference can be ascribed to the residual water content in the EA samples. Indeed, XPS is performed in ultra-high vacuum, with almost no residual water, while EA is carried out under ambient room conditions.

The zeta potentials (ζ potentials) of modified GO were measured in deionized water. The obtained values (−36.7 ± 1.4 mV for GO-C_0-βCD; −31.4 ± 0.2 mV for GO-C_2-βCD; −30.2 ± 0.1 mV for GO-C_6-βCD, −34.2 ± 2.2 mV for GO-C_{12}-βCD) were comparable to the one measured for pristine GO (−43.1 ± 2.4 mV), meaning that the experimental conditions used did not affect the surface charge. The morphology of the modified GO was studied by scanning electron microscopy (SEM). The images (Figure S5, Supporting Information) showed that GO-C_6-βCD (taken as a case study) retained the typical morphology of GO nanosheets, with a lateral size of few micrometres.

PFBA adsorption from tap water

GO-C_n-βCD nanosheets were used as sorbent of PFBA from tap water. The concentration of PFBA selected for this study was in the range of the highest ever found in surface waters (0.1–3 μg/L).[27] Adsorption kinetic studies for GO-C_n-βCD (in comparison to GAC) were carried out in batch conditions (i.e., by dispersing the material nanosheets in tap water spiked with PFBA). Figure 4a shows the removal of PFBA from tap water at different contact times (15 min, 4 h, and 24 h). For GO samples, the adsorption equilibrium occurred within 15 min, since the removal did not change at longer contact times. On the other hand, GAC showed a slower adsorption rate, reaching the maximum removal capacity after 24 h.

It should be noted that the contact time between water and GAC in a real potabilization plant is about 10–20 min. Surprisingly, among the selected case studies, only GO-C_6-βCD showed a PFBA adsorption reaching about 65% removal after only 15 min, well competing with the performance of GAC after 24 h (70% removal). Poor removal rates were found for GO and GO@βCD (removal <5%), this being likely due to the electrostatic repulsion between negatively charged GO nanosheets (ζ potential $=-43.1\pm2.4$ mV) and the anionic form of PFBA formed in tap water at neutral pH ($pK_a=0.08$–0.4).[28] Similarly to βCD free compounds, poor removal were found for GO-C_0-βCD, GO-C_2-βCD and GO-C_{12}-βCD, meaning that the amount of βCD is not the only parameter promoting the adsorption of PFBA, but a crucial role is also due to the length of the linker.

To unravel the role of the different linker length on the adsorption, molecular dynamic (MD) simulations were carried out.

MD simulations of the complexes PFBA@βCD, followed by MM-GBSA calculations (Figure S6, Supporting Information), confirmed that βCD can efficiently entrap the PFBA molecule (the binding energy of PFBA inside the βCD is -12.3 kcal mol^{-1}). Van der Waals (E_{vdw}) interactions in PFBA@βCD account for -14.3 kcal mol^{-1} and represent the driving force for the binding. The non-polar solvation term (E_{surf}), i.e., hydrophobic interactions, contributes by -2.6 kcal mol^{-1} to the total affinity, increasing the affinity of the host (βCD) for the guest (PFBA). On the other hand, the electrostatic term (E_{el}) is detrimental for the binding (4.7 kcal mol^{-1}); indeed, the charged PFBA cannot interact with water molecules while entrapped inside the hydrophobic cavity of the cyclodextrin.

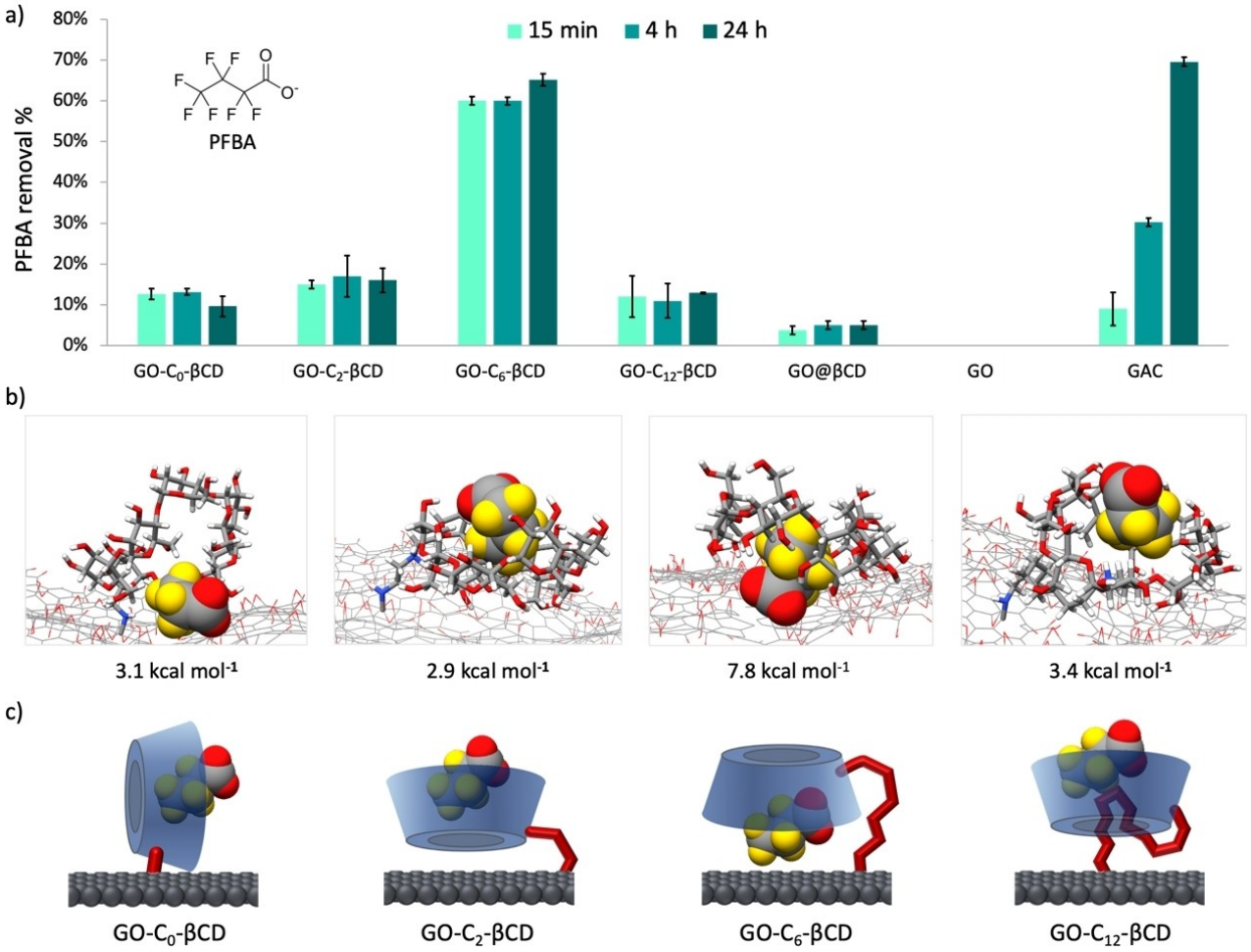

Figure 4. a) Removal of PFBA; b) binding affinity gain (kcal mol^{-1}) for PFBA and GO-C_n-βCD obtained at MM-GBSA level and representative snapshots of the MD simulations for the investigated systems; c) schematic representation of the different arrangements of βCD on GO, influencing possible complexation with PFBA. GO is in black, βCD in blue, the different linkers are in red.

Figure 4b shows the energetic gain in binding affinity of PFBA for GO-C_n-βCD (n = 0, 2, 6, and 12), due to its covalent attachment on the GO surface. This trend well-reproduces the experimental data, revealing the key role of the linker length on PFBA removal. The highest removal of PFBA by GO-C_6-βCD can be explained by assuming the formation of a "canopy-like" structure, which entraps PFBA between the GO nanosheet and the cavity of the βCD, in a sandwich-like structure. On the other hand, i) in GO-C_0-βCD the absence of the linker rigidly blocks the βCD unit perpendicular to the GO surface, restricting the possibility to interact with PFBA, ii) in GO-C_2-βCD, the βCD units lay on the surface of GO, maximising the interaction between the primary hydroxyl groups of the sugar units of the cyclodextrin and the epoxide/hydroxyl groups of GO. These interactions with the GO surface block one of the two βCD cavity portals. Finally, in GO-C_{12}-βCD the long alkyl chain of the linker shows a strong tendency to self-wrap to maximise the non-polar intramolecular interactions and to interact with the inner hydrophobic cavity of the βCD, reducing the accessibility to PFBA.

Finally, the removal of a mixture of nine PFAS (C_4–C_{13}, Figure 5) from tap water was studied. Figure 5 shows the removal after 15 min of GO and GO-C_6-βCD. Pristine GO showed high removal (> 60%) for long-chain PFAS (C_{12}–C_{14}), while resulted ineffective in the adsorption of short-chain molecules (C_4–C_8). On the other hand, GO-C_6-βCD effectively removed all nine PFAS with values ranging between 50% and 95% of removal, proving the synergic role of GO (adsorbing long-chain PFAS) and βCD (adsorbing the short-chain ones).

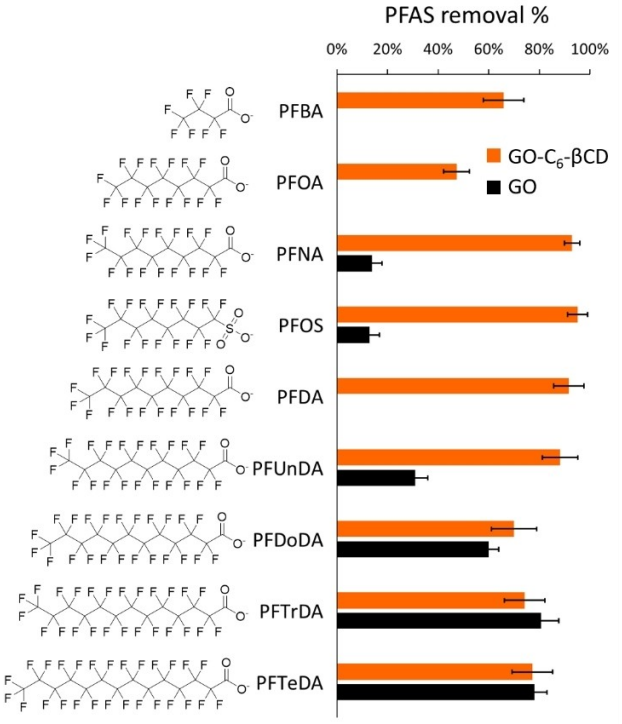

Figure 5. Removal of a mixture of PFAS after 15 min.

Conclusions

Covalent modification of GO with βCD was realized by epoxide ring opening reaction through amino-ended βCD. Tailored alkyl chains with length in the range C_0-C_{12} were exploited as linkers between GO and βCD. The reaction enabled loadings in the range 12–36% and negligible reduction of GO precursor. Covalent binding was demonstrated by comparing ATR-FTIR, TGA, XPS and EA of GO-C_n-βCD to those of two control samples and by the PFBA adsorption test results. Poor adsorption efficiencies were indeed found for control samples. Moreover, the adsorption was not only related to the presence/amount of βCD but mainly to the length of the alkyl linkers. A removal up to 65% after just 15 min was found for GO-C_6-βCD only. Molecular dynamic simulations ascribed the observed trend to the complexation of PFBA in the βCD cavity (occurring in all of the GO-C_n-βCD materials tested) and synergic entrapping of PFBA between the GO nanosheet and the cavity of the βCD in a sandwich-like structure, peculiar to the C_6 linker. Remarkably, GO-C_6-βCD outperformed GAC (industrial sorbent benchmark) at short contact time and well compares with the adsorption of GAC after 24 h. The adsorption synergy of GO and βCD was finally proved for a mixture of PFAS of different fluoroalkyl chain length. Long-chain PFAS were well adsorbed by GO and short-chain ones were retained by the CD unit, this revealing great potential of the presented approach for drinking water purification from emerging contaminants. Future studies will focus on the exploitation of GO-C_6-βCD for engineering technologies, such as membranes, for PFAS removal under flow conditions.

Experimental Section

Materials

GO powder was purchased from Layer One (Norway, previously Abalonyx) and used without further purification (graphene oxide dry powder < 35 mesh, product code 1.8). Before using, GO was sonicated in ultrapure water to exfoliate the bulk material into monolayer (> 99%) with lateral size of few micrometers.[12b,29] GAC was purchased from CABOT Norit Spa (Ravenna, Italy, Norit GAC 830 AF, MB index min 240 mg/g, BET surface area > 1000 m^2/g) and use without further purification. PFAS standards were purchased by Agilent Technologies (Santa Clara, CA, US). The experiments on PFAS were carried out by using polypropylene vials. All other chemicals were purchased from Sigma Aldrich or Termo Fisher and used without any further purification. Purification of modified GO was performed by using microfiltration modules Plasmart 100 MF modules (Versatile® PES hollow fibers, membrane area filtering surface 0.1 m^2, pore average size 100–200 nm) were provided by Medica Spa (Medolla, Italy).

Synthesis of modified β-cyclodextrins

Firstly, tosyl-βCD was obtained by following the procedure reported by Ohashi et al.,[18b] with some modifications (Scheme 1a).

βCD (5 g; 4.4 mmol) and toluenesulfonyl chloride (TsCl, 3.75 g; 19.6 mmol) were dissolved in an aqueous sodium hydroxide solution (0.4 M, 75 mL) and reacted under vigorous stirring at 0 °C

for 1 h. Unreacted TsCl was filtered off, hydrochloric acid was used to neutralize the solution and unrefined tosyl-βCD was obtained as precipitate. 1.2 g of pure tosyl-βCD were obtained from recrystallization of the crude from hot water (90 °C, 25 mL).

C_0-βCD was obtained by following a two-steps reaction reported by Bonnet et al.,[18a] with some modifications (Scheme 1a).

Tosyl-βCD (1 g; 0.78 mmol) was suspended in deionized water (10 mL) and sodium azide (0.65 g; 0.01 mmol) was added. The reaction was carried out under stirring at 80 °C for 5 h. After cooling to room temperature, acetone (60 mL) was added, and the resulting precipitate was vacuum-dried to obtain 0.9 g of azide-βCD (N_3-βCD).

N_3-βCD (540 mg; 0.466 mmol) and triphenylphosphine (206 mg; 0.785 mmol) were dissolved in dimethylformamide (10 mL) and NH_3 (2 mL, 28% aqueous solution) was added. The mixture was stirred at room temperature for 12 h, then acetone (80 mL) was added to obtain the crude product as a white precipitate. To remove by-products, the crude was dissolved in a small quantity of DMF and then precipitated from acetone to obtained 440 mg of C_0-βCD.

C_2-βCD, C_6-βCD and C_{12}-βCD were obtained by following the procedure reported by Ohashi et al.,[18b] with some modifications (Scheme 1a).

Tosyl-βCD (0.5 g; 0.39 mmol) was added in 1,2-ethylenediamine (5.8 mL) or 1,6-hexamethylenediamine (6 g) or 1,12-dodecanediamine (6 g) and stirred at 70 °C for 6 h. The unreacted diamine was removed washing several times with acetone and the obtained white powder was dissolved in a mixture of methanol:water (3:1) by heating and reprecipitation from acetone. The filtered product was washed with acetone to obtain a white solid (C_2-βCD, C_6-βCD and C_{12}-βCD).

Synthesis and purification of GO-C_n-βCD

100 mg of GO were dispersed in 30 mL of deionized water:EtOH (1:1) and sonicated for 2 h, then a solution of C_0-βCD, C_2-βCD, C_6-βCD or C_{12}-βCD (200 mg in 100 mL of deionized water and EtOH in ratio 1:1) was added under vigorous stirring. The mixture was refluxed overnight, then the crude was purified by microfiltration on commercial Plasmart 100 modules (Medica s.p.a.) accordingly to previously reported procedures.[12d] A total volume of about 1 L of water was required to purify the crude. The suspension was freeze-dried to obtain about 140 mg of GO-C_n-βCD (n = 0, 2, 6, 12). The first control material (GO@βCD) was prepared with the same procedure using commercial βCD (without alkyl linker). The second control material (GO-control) was prepared under the same experimental conditions without the addition of βCD.

Characterization

ATR FTIR spectra were recorded with Agilent Cary 630 FTIR Spectrophotometer, and the spectra are expressed by wavenumber (cm^{-1}).

Thermogravimetric analyses were recorded with PerkinElmer Thermogravimetric Analyzer TGA 4000 by PerkinElmer, in air atmosphere, from 30 °C to 800 °C, with a scanning temperature of 10 °C/min.

High-resolution XPS was performed using a Phoibos 100 hemispherical energy analyser, using Mg K_α radiation ($\hbar\omega$ = 1,253.6 eV; X-ray power = 125 W) in constant analyser energy (CAE) mode, with analyser pass energies of 10 eV. Base pressure in the analysis chamber during analysis was 4.2×10^{-8} mbar. Spectra were fitted by using CasaXPS (www.casaxps.com) after Shirley background subtraction and all spectra were calibrated to the C1s binding energy (285.0 eV). XPS samples were tablet prepared from the dry powder of each material and fixing it on the sample holder by conductive carbon tape.

Elemental analysis was performed on powder materials by using an Elementar Unicube Elemental analyser, method GRAPHITE.

ζ potential was measured in deionized water, using NanoBrook Omni Particle Size Analyzer.

Scanning electron microscopy (SEM) analyses were performed with a ZEISS LEO 1530 FEG. The samples were deposited on a cleaned silicon wafer by dropping 10 μL of suspension at 0.05 mg/mL in dimethylformamide. The energy of electrons was 5 keV and the signal was acquired using an in Lens detector at a working distance of 3–5 mm.

NMR spectra were recorded with a Varian Mercury 400 Spectrometer (400 MHz for ^{1}H NMR and 100 MHz for ^{13}C NMR spectra) and Agilent NMR Spectrometer 500 MHz (500 MHz for ^{1}H NMR, and 125 MHz for ^{13}C NMR spectra). The chemical shifts (δ) are reported in parts per million (ppm) referred to the signals of the residual solvents (^{1}H $CHCl_3$ = 7.26 ppm; DMSO = 2.48 ppm and H_2O = 4.79 ppm; ^{13}C $CHCl_3$ = 77.0 ppm and DMSO = 40.0 ppm). Coupling constants (J) are reported in Hz and multiplicity are named by the following abbreviations: singlet (s), doublet (d), double of doublets (dd), triplet (t), multiplet (m), broad (b).

Adsorption experiments

25 mg of powder materials (GO, GO-C_0-βCD, GO-C_2-βCD, GO-C_6-βCD, GO-C_{12}-βCD, GO@βCD) were sonicated in 10 mL of ultrapure water for 2 h to exfoliate the bulk material into monolayer nanosheets.[29] After sonication, tap water (15 mL) and PFBA (125 μL of a stock solution of 100 μg/L in MeOH) were added to the suspensions to obtain a final concentration of 0.5 μg/L in a final volume of 25 mL. For non-powder materials (i.e., GAC), 25 mg of samples were directly added to 25 mL of tap water and 125 μL of PFBA (100 μg/L in MeOH) to obtain a final concentration of 0.5 μg/L. Samples were then left under gentle agitation for 15 min, 4 h and 24 h, then each sample was centrifuged (10 min, 10,000 rpm) and analyzed with UPLC-MS/MS.

PFAS adsorption test were performed using the same experimental conditions. Nine selected PFAS were added to the suspension to reach a final concentration of 0.5 μg/L of each contaminants and samples were left under gentle agitation for 15 min.

PFAS quantification

Samples containing PFAS were analyzed by UPLC-MS/MS (ACQUITY UPLC H-Class PLUS – XEVO TQS Micro mass detector, Waters). 1 mL samples were used as sources for the automated injection. The chromatographic separation was performed on a reverse phase Waters Acquity UPLC CSH Phenyl-Hexyl (1.7 μm, 2.1×100 mm) column and Waters Isolator Column (2.1×50 mm). The column temperature was 34 °C, the flow rate 0.3 mL/min and the injection volume 40 μL, while the total run time was 8 min for PFBA and 21 min for the mixture of nine PFAS. The mobile phase consisted of a biphasic gradient, NH_4OAc 2 mM in a mixture of ultrapure water: methanol 95:5 as phase A, and NH_4OAc 2 mM in MeOH as phase B. The mobile phase composition varied according to the gradient program reported in Tables S3 and S4. Mass details and the transitions monitored are reported in Tables S5 and S6.

Molecular dynamics simulations

The model-systems representing GO-C_n-βCD (n = 0, 2, 6 and 12) were created on a pristine graphene sheet, generated by VMD, of dimensions 4 nm ×4 nm. Based on the atomic composition obtained by XPS, reported in Table 1, oxygen-containing groups (epoxy, hydroxyl, carbonyl and carboxyl) were randomly positioned on the surface, employing the GO-py program. PFAS, βCD, and GO-C_n-βCD were described by the General Amber Force Field (GAFF) force field. The atomic charges were obtained at AM1 level of theory. The systems were fully solvated using TIP3P water molecules, and counterions (necessary to neutralize the total charge of the complexes) were added. All the systems were initially minimized and equilibrated and then 100 ns MD simulations were carried out. Amber16 software was used to perform all the simulation herein reported. The affinities of the PFBA for βCD and GO-C_n-βCD were computed by the Molecular Mechanics-Generalized Born Surface Area (MM-GBSA) algorithm, as implemented in Amber16.

Author Contributions

F. Tunioli: Methodology, Investigation. T. D. Marforio: Investigation, Conceptualization. L. Favaretto: Methodology, Investigation. S. Mantovani: Methodology. A. Pintus: Methodology. A. Bianchi: Methodology, Investigation. A. Kovtun: Investigation, Formal analysis. M. Agnes: Investigation. V. Palermo: Conceptualization, Validation. M. Calvaresi: Investigation, Conceptualization. M. L. Navacchia: Investigation, Formal analysis. M. Melucci: Conceptualization, Validation, Writing – original draft.

Acknowledgements

The authors gratefully acknowledge the support of this work by the projects Life-Remembrance, ENV/IT/001001 Life Resource and Environment LIFE20 'Give plastic wastes from the production of hollow-fiber membranes a second life', project 881603-GrapheneCore3-H2020-SGA-FET- SH1 Graphil- GRAPHENE-FLAGSHIP and PRIN 2017 W8KNZW_002 'New Approaches in Nanocarbo-catalysis for organic transformations (NANO-CARBO-CAT)'.

Conflict of Interests

The authors declare no conflict of interest.

Data Availability Statement

The data that support the findings of this study are available in the supplementary material of this article.

Keywords: adsorption · β-cyclodextrins · emerging contaminants · graphene oxide · water purification

[1] a) M. F. Rahman, S. Peldszus, W. B. Anderson, *Water Res.* **2014**, *50*, 318–340; b) S. Kancharla, P. Alexandridis, M. Tsianou, *Curr. Opin. Colloid Interface Sci.* **2022**, *58*, 101571; c) M. G. Evich, M. J. B. Davis, J. P. McCord, B. Acrey, J. A. Awkerman, D. R. U. Knappe, A. B. Lindstrom, T. F. Speth, C. Tebes-Stevens, M. J. Strynar, Z. Wang, E. J. Weber, W. M. Henderson, J. W. Washington, *Science* **2022**, *375*, eabg9065.

[2] a) F. Li, J. Duan, S. Tian, H. Ji, Y. Zhu, Z. Wei, D. Zhao, *Chem. Eng. J.* **2020**, *380*, 122506; b) S. P. Lenka, M. Kah, L. P. Padhye, *Water Res.* **2021**, *199*, 117187.

[3] J. T. Thompson, B. Chen, J. A. Bowden, T. G. Townsend, *Env. Sci. Technol. Lett.* **2023**, *10*, 234–239.

[4] a) G. Bertanza, G. U. Capoferri, M. Carmagnani, F. Icarelli, S. Sorlini, R. Pedrazzani, *Sci. Total Environ.* **2020**, *734*, 139154; b) G. Pitter, F. D. Re, C. Canova, G. Barbieri, M. Z. Jeddi, F. Daprà, F. Manea, R. Zolin, A. M. Bettega, G. Stopazzolo, S. Vittorii, L. Zambelli, M. Martuzzi, D. Mantoan, F. Russo, *Environ. Health Perspect.* **2020**, *128*, 027007; c) M. Mastrantonio, E. Bai, R. Uccelli, V. Cordiano, A. Screpanti, P. Crosignani, *Eur. J. Public Health* **2017**, *28*, 180–185.

[5] a) Y. Xu, C. Nielsen, Y. Li, S. Hammarstrand, E. M. Andersson, H. Li, D. S. Olsson, K. Engström, D. Pineda, C. H. Lindh, T. Fletcher, K. Jakobsson, *Environ. Int.* **2021**, *147*, 106333; b) S. Banzhaf, M. Filipovic, J. Lewis, C. J. Sparrenbom, R. Barthel, *Ambio* **2017**, *46*, 335–346.

[6] a) J. Hölzer, T. Göen, K. Rauchfuss, M. Kraft, J. Angerer, P. Kleeschulte, M. Wilhelm, *Int. J. Hyg. Environ. Health* **2009**, *212*, 499–504; b) S. Takagi, F. Adachi, K. Miyano, Y. Koizumi, H. Tanaka, M. Mimura, I. Watanabe, S. Tanabe, K. Kannan, *Chemosphere* **2008**, *72*, 1409–1412; c) C. Eschauzier, E. Beerendonk, P. Scholte-Veenendaal, P. De Voogt, *Environ. Sci. Technol.* **2012**, *46*, 1708–1715; d) C. Flores, F. Ventura, J. Martin-Alonso, J. Caixach, *Sci. Total Environ.* **2013**, *461–462*, 618–626.

[7] a) E. Gagliano, M. Sgroi, P. P. Falciglia, F. G. A. Vagliasindi, P. Roccaro, *Water Res.* **2020**, *171*, 115381; b) Z. Du, S. Deng, Y. Bei, Q. Huang, B. Wang, J. Huang, G. Yu, *J. Hazard. Mater.* **2014**, *274*, 443–454.

[8] http://www.chemsafetypro.com/Topics/EU/REACH_Regulation_EC_No_1907_2006.html.

[9] J. Yuan, S. Mortazavian, E. Passeport, R. Hofmann, *Sci. Total Environ.* **2022**, *838*, 156406.

[10] N. Belkouteb, V. Franke, P. McCleaf, S. Köhler, L. Ahrens, *Water Res.* **2020**, *182*, 115913.

[11] a) N. Baig, Ihsanullah, M. Sajid, T. A. Saleh, *J. Environ. Manage.* **2019**, *244*, 370–382; b) G. Ersan, O. G. Apul, F. Perreault, T. Karanfil, *Water Res.* **2017**, *126*, 385–398.

[12] a) S. Khaliha, T. D. Marforio, A. Kovtun, S. Mantovani, A. Bianchi, M. Luisa Navacchia, M. Zambianchi, L. Bocchi, N. Boulanger, A. lakunkov, M. Calvaresi, A. V. Talyzin, V. Palermo, M. Melucci, *FlatChem* **2021**, *29*, 100283; b) S. Khaliha, A. Bianchi, A. Kovtun, F. Tunioli, A. Boschi, M. Zambianchi, D. Paci, L. Bocchi, S. Valsecchi, S. Polesello, A. Liscio, M. Bergamini, M. Brunetti, M. Luisa Navacchia, V. Palermo, M. Melucci, *Sep. Purif. Technol.* **2022**, *300*, 121826; c) S. Mantovani, S. Khaliha, L. Favaretto, C. Bettini, A. Bianchi, A. Kovtun, M. Zambianchi, M. Gazzano, B. Casentini, V. Palermo, M. Melucci, *Chem. Commun.* **2021**, *57*, 3765–3768; d) S. Mantovani, S. Khaliha, T. D. Marforio, A. Kovtun, L. Favaretto, F. Tunioli, A. Bianchi, G. Petrone, A. Liscio, V. Palermo, M. Calvaresi, M. L. Navacchia, M. Melucci, *Chem. Commun.* **2022**, *58*, 9766–9769; e) S. Mantovani, T. D. Marforio, S. Khaliha, A. Pintus, A. Kovtun, F. Tunioli, L. Favaretto, A. Bianchi, M. L. Navacchia, V. Palermo, M. Calvaresi, M. Melucci, *Environ. Sci.: Water Res. Technol* **2023**, *9*, 1030.

[13] a) M. Zambianchi, S. Khaliha, A. Bianchi, F. Tunioli, A. Kovtun, M. L. Navacchia, A. Salatino, Z. Xia, E. Briñas, E. Vázquez, D. Paci, V. Palermo, L. Bocchi, B. Casentini, M. Melucci, *J. Membr. Sci.* **2022**, *658*, 120707; b) M. Zambianchi, M. Durso, A. Liscio, E. Treossi, C. Bettini, M. L. Capobianco, A. Aluigi, A. Kovtun, G. Ruani, F. Corticelli, M. Brucale, V. Palermo, M. L. Navacchia, M. Melucci, *J. Chem. Eng.* **2017**, *326*, 130–140.

[14] A. Kovtun, A. Bianchi, M. Zambianchi, C. Bettini, F. Corticelli, G. Ruani, L. Bocchi, F. Stante, M. Gazzano, T. D. Marforio, M. Calvaresi, M. Minelli, M. L. Navacchia, V. Palermo, M. Melucci, *Faraday Discuss.* **2021**, *227*, 274–290.

[15] a) S. Wacławek, K. Krawczyk, D. Silvestri, V. V. T. Padil, M. Řezanka, M. Černík, M. Jaroniec, *Adv. Colloid Interface Sci.* **2022**, *310*, 102807; b) B. Tian, S. Hua, Y. Tian, J. Liu, *Environ. Sci. Pollut. Res. Int.* **2021**, *28*, 1317–1340; c) Q. Liu, Y. Zhou, J. Lu, Y. Zhou, *Chemosphere* **2020**, *241*, 125043; d) K. Köse, M. Tüysüz, D. Aksüt, L. Uzun, *Environ. Sci. Pollut. Res. Int.* **2022**, *29*, 182–209; e) S. E. Z. Syeda, D. Nowacka, M. S. Khan, A. M. Skwierawska, in *Polymers, Vol. 14*, **2022**, p. 2341; f) A. H. Karoyo, L. D. Wilson, *J. Colloid Interface Sci.* **2013**, *402*, 196–203; g) H. Takezawa, T. Murase, G. Resnati, P. Metrangolo, M. Fujita, *J. Am. Chem. Soc.* **2014**, *136*, 1786–1788; h) A. H. Karoyo, L. D. Wilson, *Nanomaterials* **2015**, *5*, 981–

1003; i) A. Yang, C. Ching, M. Easler, D. E. Helbling, W. R. Dichtel, *ACS Materials Lett.* **2020**, *2*, 1240–1245.
[16] M. J. Weiss-Errico, K. E. O'Shea, *J. Inclusion Phenom. Macrocyclic Chem.* **2019**, *95*, 111–117.
[17] I. A. Vacchi, C. Spinato, J. Raya, A. Bianco, C. Ménard-Moyon, *Nanoscale* **2016**, *8*, 13714–13721.
[18] a) V. Bonnet, R. Duval, V. Tran, C. Rabiller, *Eur. J. Org. Chem.* **2003**, *24*, 4810–4818; b) H. Ohashi, Y. Hiraoka, T. Yamaguchi, *Macromolecules* **2006**, *39*, 2614–2620.
[19] L. Fu, G. Lai, A. Yu, *RSC Adv.* **2015**, *5*, 76973–76978.
[20] M. B. Clark, J. A. Gardella, T. M. Schultz, D. G. Patil, L. Salvati, *Anal. Chem.* **1990**, *62*, 949–956.
[21] R. A. Zangmeister, T. A. Morris, M. J. Tarlov, *Langmuir* **2013**, *29*, 8619–8628.
[22] A. Artemenko, A. Shchukarev, P. Štenclová, T. Wågberg, J. Segervald, X. Jia, A. Kromka, *Iop. Conf. Ser. Mater. Sci. Eng.* **2021**, *1050*, 012001.
[23] J. Russat, *Surf. Interface Anal.* **1988**, *11*, 414–420.
[24] J. Liebscher, R. Mrówczyński, H. A. Scheidt, C. Filip, N. D. Hădade, R. Turcu, A. Bende, S. Beck, *Langmuir* **2013**, *29*, 10539–10548.
[25] P. Louette, F. Bodino, J.-J. Pireaux, *Surf. Sci. Spectra* **2006**, *12*, 12–17.
[26] R. Shibuya, K. Takeyasu, D. Guo, T. Kondo, J. Nakamura, *Langmuir* **2022**, *38*, 14430–14438.
[27] a) P. Wang, Y. Lu, T. Wang, Z. Zhu, Q. Li, J. Meng, H. Su, A. C. Johnson, A. J. Sweetman, *Environ. Pollut.* **2016**, *218*, 1234–1244; b) X. Cao, C. Wang, Y. Lu, M. Zhang, K. Khan, S. Song, P. Wang, C. Wang, *Ecotoxicol. Environ. Saf.* **2019**, *174*, 208–217.
[28] A. H. Karoyo, P. Sidhu, L. D. Wilson, P. Hazendonk, *J. Phys. Chem. B* **2013**, *117*, 8269–8282.
[29] A. Liscio, K. Kouroupis-Agalou, X. D. Betriu, A. Kovtun, E. Treossi, N. M. Pugno, G. De Luca, L. Giorgini, V. Palermo, *2D Mater.* **2017**, *4*, 025017.

Manuscript received: June 9, 2023
Accepted manuscript online: August 7, 2023
Version of record online: September 19, 2023